Characterization of Hyperinsulinism in Infancy Assessed with PET and ^{18}F-Fluoro-L-DOPA

Maria-João Ribeiro, MD, PhD[1]; Pascale De Lonlay, MD, PhD[2]; Thierry Delzescaux, PhD[1]; Nathalie Boddaert, MD[3]; Francis Jaubert, MD[4]; Sandrine Bourgeois[1]; Frédéric Dollé, PhD[1]; Claire Nihoul-Fékété, MD[5]; André Syrota, MD, PhD[1]; and Francis Brunelle, MD[3]

[1]Service Hospitalier Frédéric Joliot, Département de Recherche Médicale, Direction des Sciences du Vivant, Commissariat à l'Energie Atomique, Orsay, France; [2]Département de Métabolisme et Pédiatrie, Hôpital Necker-Enfants Malades, Paris, France; [3]Service de Radiologie Pédiatrique, Hôpital Necker-Enfants Malades, Paris, France; [4]Laboratoire de Anatomopathologie, Hôpital Necker-Enfants Malades, Paris, France; and [5]Département de Chirurgie Infantile, Hôpital Necker-Enfants Malades, Paris, France

Hyperinsulinism (HI) of infancy is a neuroendocrine disease secondary to either focal adenomatous hyperplasia or a diffuse abnormality of insulin secretion of the pancreas. HI with focal lesions can revert by selective surgical resection in contrast to the diffuse form, which requires subtotal pancreatectomy when resistant to medical treatment. Neuroendocrine diseases are a heterogeneous group of entities with the ability to take up amine precursors and to convert them into biogenic amines. Therefore, the aim of this study was (a) to evaluate the use of PET with ^{18}F-fluoro-L-dihydroxyphenylalanine (^{18}F-fluoro-L-DOPA) and (b) to distinguish between focal and diffuse HI. **Methods:** Fifteen patients (11 boys, 4 girls) with neonatal HI were enrolled in this study. All patients fasted for at least 6 h before the PET examination and their medication was discontinued for at least 72 h. The examination was performed under light sedation (pentobarbital associated with or without chloral). The dynamic acquisition started 45–65 min after the injection of ^{18}F-fluoro-L-DOPA (4.0 MBq/kg weight). Four or 6 scans of 5 min each (2 or 3 steps according to the height of the patient) were acquired from the neck to the upper legs. **Results:** An abnormal focal pancreatic uptake of ^{18}F-fluoro-L-DOPA was observed in 5 patients, whereas a diffuse uptake of the radiotracer was observed in the pancreatic area of the other patients. All patients with focal radiotracer uptake and also 4 of 10 patients with pancreatic diffuse radiotracer accumulation, unresponsive to medical treatment, underwent surgery. The histopathologic results confirmed the PET findings—that is, focal versus diffuse HI. **Conclusion:** The results of this study suggest that ^{18}F-fluoro-L-DOPA could be an accurate noninvasive technique to distinguish between focal and diffuse forms of HI.

Key Words: hyperinsulinism of infancy; PET; ^{18}F-fluoro-L-DOPA

J Nucl Med 2005; 46:560–566

Hyperinsulinism (HI) is the most important cause of recurrent hypoglycemia in infancy. The hypersecretion of insulin induces profound hypoglycemias that require aggressive treatment to prevent the high risk of neurologic complications (*1,2*). HI can be due to 2 different histopathologic types of lesions, a focal or a diffuse form (*3,4*), based on different molecular entities despite an indistinguishable clinical pattern (*5–9*). In focal HI, which represents about 40% of all cases (*10*), the pathologic pancreatic β-cells are gathered in a focal adenoma, usually 2.5–7.5 mm in diameter. Conversely, diffuse HI corresponds to an abnormal insulin secretion of the whole pancreas with disseminated β-cells showing enlarged abnormal nuclei (*11*). Finally, about 10% of HI cases are clinically atypical and cannot be classified, having an unknown molecular basis and histopathologic form (*12*).

Control of HI is attempted through medical treatment with diazoxide, nifedipine, or octreotide (*13–15*), but pancreatectomy is the only issue for patients who are resistant to these treatments (*10,16*). Therefore, the differential diagnosis between the 2 forms becomes of major importance since their surgical treatment and the outcome differ considerably. Focal HI is totally cured by selective resection of the adenoma, whereas diffuse forms of HI require a subtotal pancreatectomy, with severe iatrogenic diabetes as a consequence (*17,18*).

The localization of insulin hypersecretion before surgery is possible only through pancreatic venous catheterization (PVS), allowing a pancreatic map of insulin concentrations, with an eventual additional pancreatic arterial calcium stimulation (*19–21*). PVS is an invasive method, which is technically difficult to perform and requires general anesthesia. The concentrations of plasmatic glucose must be maintained between 2 and 3 mmol/L before and during PVS. Moreover, all medical treatments must be stopped 5 d before the study. Therefore, it is of major interest to find a less invasive way to differentiate between focal and diffuse HI. This method

Received Sep. 9, 2004; revision accepted Dec. 15, 2004.

For correspondence or reprints contact: Maria-João Ribeiro, MD, PhD, Service Hospitalier Frédéric Joliot, DRM/DSV, CEA, 4, place du Général Leclerc, F-91406 Orsay, France.

E-mail: ribeiro@shfj.cea.fr

should precisely localize the pathologic area of focal HI to guide the surgeon.

L-Dihydroxyphenylalanine (L-DOPA) is a precursor of catecholamines that is converted to dopamine by the aromatic amino acid decarboxylase (AADC). In addition to its role as a precursor of noradrenaline and adrenaline, dopamine is a transmitter substance in the central and peripheral nervous system. The capacity to take up and decarboxylate amine precursors such as L-DOPA and 5-hydroxytryptophan and to store their biogenic amine (dopamine and serotonin) is characteristic of neuroendocrine cells.

Pancreatic cells contain markers usually associated with neuroendocrine cells, such as tyrosine hydroxylase, dopamine, neuronal dopamine transporter, vesicular dopamine transporter, and monoamine oxidases A and B (*22–24*). Pancreatic islets have been shown to take up L-DOPA and convert it to dopamine through the AADC (*25–27*).

PET performed with ^{18}F-fluoro-L-dihydroxyphenylalanine (^{18}F-fluoro-L-DOPA) has been extensively used to study the central dopaminergic system. Nevertheless, several recent studies have demonstrated the usefulness of this radiotracer to detect neuroendocrine tumors such as pheochromocytomas, thyroid medullar carcinomas, or gastrointestinal carcinoid tumors that usually contain secretory granules and have the ability to produce biogenic amines (*28,29*).

The aim of this work was to evaluate the use of whole-body PET with ^{18}F-fluoro-L-DOPA to detect the hyperfunctional pancreatic islet tissue and to test its ability to differentiate between focal and diffuse HI.

MATERIALS AND METHODS

Patients

Fifteen patients (11 boys, 4 girls; age range, 1–14 mo; mean age ± SD, 5.7 ± 3.8 mo) with neonatal HI were studied with ^{18}F-fluoro-L-DOPA and PET (Table 1). In all cases, HI diagnosis was based on persistent hypoglycemia with low plasma ketone bodies and free fatty acids together with measurable circulating insulin levels at the time of hypoglycemia.

All patients fasted for at least 6 h before the PET study and their medications were stopped for at least 72 h. Two patients had 2 scans. One patient had a PET study before and after treatment with an inhibitor of AADC (L-α-hydrazino-α-methyl-β-(3,4-dihydroxyphenyl)propionic acid or carbidopa). Another patient had a PET study 72 h after drug withdrawal and another PET study after administration of octreotide and diazoxide. During all PET studies, normoglycemia was maintained by glucose infusion, which was carefully adjusted according to frequent blood glucose monitoring. Maximal glucose infusion rates between 6.4 and 13.2 mg/kg/min were needed. PET acquisition was performed under light sedation (pentobarbital associated with or without chloral).

The 5 patients for whom ^{18}F-fluoro-L-DOPA uptake results strongly suggested focal HI and the patients with diffuse HI resistant to medical treatment (n = 4/10) underwent surgery. Pancreatic tissue obtained from surgical resections was fixed in formalin and embedded in paraffin, and serial sections were studied by immunohistochemistry after a water bath antigen retrieval step. The primary antibodies used were antiproinsulin (1/400 mouse monoclonal antibody, 1G4; Novocastra), antichromogranin A (1/200 mouse monoclonal antibody DAK-A3; DAKO), antisynaptophysin (1/50 rabbit polyclonal antibody A0010; DAKO), and anti-DOPA decarboxylase or anti-AADC (1/100 rabbit polyclonal antibody; Chemicon International).

TABLE 1
Clinical Profile of 15 Patients with HI

Patient no.	Sex	Birth weight (g)	Gestational age (wk)	Age (mo)		Weight at PET scan (g)	Response to medication	Surgery
				At diagnosis	At PET scan			
1	M	3,470	36	Neonatal	5	7,500	Dzx−, Octr−	Yes
2	M	3,760	40	Neonatal	3	5,800	Dzx−, Octr−	Yes
3	F	3,310	38	Neonatal	2	5,000	Dzx−, Octr−	Yes
4	M	3,871	38	Neonatal	4	9,160	Dzx−, Octr−	Yes
5	M	4,050	37	Neonatal	7	10,870	Dzx−, Octr+	Yes
6	M	4,450	38	Neonatal	4	8,190	Dzx−, Octr−	Yes
7	M	3,690	36	Neonatal	5	8,600	Dzx−, Octr+	No
8	M	3,900	39	Neonatal	3 and 12	6,800 10,680	Dzx−, Octr+	No
9	F	2,950	37	2.5	13	11,000	Dzx+	No
10	F	4,010	37	Neonatal	8	7,300	Dzx−, Octr+	No
11	F	3,480	37	Neonatal	5	6,070	Dzx−, Octr−	Yes
12	M	5,000	38	Neonatal	14 and 17	11,500 12,200	Dzx−, Octr−	Yes
13	M	3,700	38	Neonatal	2	6,670	Dzx−, Octr+	No
14	M	3,800	38	Neonatal	9	9,800	Dzx−, Octr+	No
15	M	3,580	36	Neonatal	2	6,000	Dzx−, Octr−	Yes

Dzx = diazoxide; Octr = octreotide.

Data Acquisition

MRI. Six patients underwent MRI of the abdomen before or after the PET study, using a 1.5-T imager (Signa; General Electric). T1-weighed SPGR (spoiled gradient acquisition at the steady state) acquisition with inversion recovery was performed to allow 3-dimensional (3D) reconstruction of MR images. MRI was used to reveal potential signal abnormalities in the pancreas and to allow the coregistration between PET and MRI.

PET. The PET studies were performed using an ECAT EXACT HR+ scanner (Siemens/CTI) that collects 63 simultaneous 2.4-mm-thick slices with an intrinsic in-plane resolution of 4.3 mm. The patients were placed in supine position in the tomograph using a 3D laser alignment. To ensure the optimal position in the scanner and to avoid movement artifacts, the children were comfortably immobilized during the study acquisition by placing them in a vacuum mattress. The synthesis of ^{18}F-fluoro-L-DOPA followed a previously described electrophilic procedure (*30*). Intravenous bolus injection of ^{18}F-fluoro-L-DOPA (a mean of 4.0 MBq/kg weight) was done 30–50 min before transmission acquisition.

Tissue attenuation was measured using three ^{68}Ge rod sources (approximately 450 MBq). Transmission scans (2-dimensional acquisition mode) lasted 2.5 min per bed position (field of view [FOV] of 15 cm), with 2 or 3 steps, according to the height of the patient, from the neck to the hip. After segmentation, the transmission scans were used for subsequent correction of attenuation of emission scans. Thorax–abdomen emission scans (3D acquisition mode) starting 45–65 min after the radiotracer injection (2.5-min step acquisition, 2 or 3 steps for 1 scan) were acquired over 30 min.

Data Analysis

The emission sets were corrected for scatter using a model-based correction, allowing the simulation of the map of single scatter events. The images were reconstructed using an attenuation-weighted ordered-subset expectation maximization iterative algorithm with 4 iterations and 6 subsets. The final spatial resolution in reconstructed images was approximately 6.0 mm.

The reconstructed images were evaluated in a 3D display using axial, coronal, and sagittal views to visualize the pancreas, which always presented a high uptake of ^{18}F-fluoro-L-DOPA, and to distinguish it from the surrounding organs in the abdomen.

For each patient, all thorax–abdomen emission scans were assembled with bed position overlap, and this integrated image was used to define regions of interest (ROIs) over the pancreas, liver, kidneys, and lungs. The mean activity concentration value in each ROI was calculated and used to generate regional time–activity curves. These curves were used to evaluate the contrast between the pancreas and other tissues and the biologic clearance of ^{18}F-fluoro-L-DOPA.

The mean activity concentration measured in each ROI, 60 min after injection, was used to calculate standardized uptake values (SUVs). The mean radioactivity concentration in each ROI was divided by the injected dose of ^{18}F-fluoro-L-DOPA (corrected to the beginning of the emission acquisition) and the body weight. Based on visual analysis, the patient's HI was classified in 2 groups, focal or diffuse, and quantitatively compared using the SUVs. Comparisons were done using an ANOVA test for repeated measures.

The assembled image was also used to achieve the coregistration with MRI slices. With regard to MRI acquisitions, a specific FOV was determined to include the pancreas, liver, and kidneys, which were the only organs visible in PET images in the abdominal area. A corresponding FOV was then extracted from PET images. Due to the low contrast observed between kidneys and surrounding organs on MR images, an enhancement of the gray level intensity of these structures based on a manual segmentation of the kidneys was performed. Volume-based coregistration of PET and enhanced MR images were done using mutual information as the matching criterion (*31–33*). Global rigid transformation was considered for the spatial alignment (*34*). The coregistration task was evaluated visually using a fusion mode taking into account the superimposition of the liver and the kidneys in both modalities (*35*). Finally, the improvement of pancreatic uptake targeting on the pancreas was achieved by fusing anatomic MRI and functional coaligned PET information on the pancreas.

RESULTS

The 6 pancreatic MR images were normal and, therefore, noninformative concerning the difference between focal and diffuse HI.

The PET images showed that most of the radioactivity injected was found in the kidneys and urinary bladder (Figs. 1A, 2A, and 2B). Variable uptakes were also seen in the liver, gallbladder, biliary duct, and duodenum, all of which could be discerned from the pancreas. In 5 of 15 patients, a focal uptake (hot spot) of ^{18}F-fluoro-L-DOPA was observed in the pancreatic area (Fig. 1A, patient 3). The focal localization was the head of the pancreas ($n = 4$) and in 1 patient in the body. The 5 patients with a focal increase of the radiotracer uptake underwent a limited pancreatic resection that was followed by

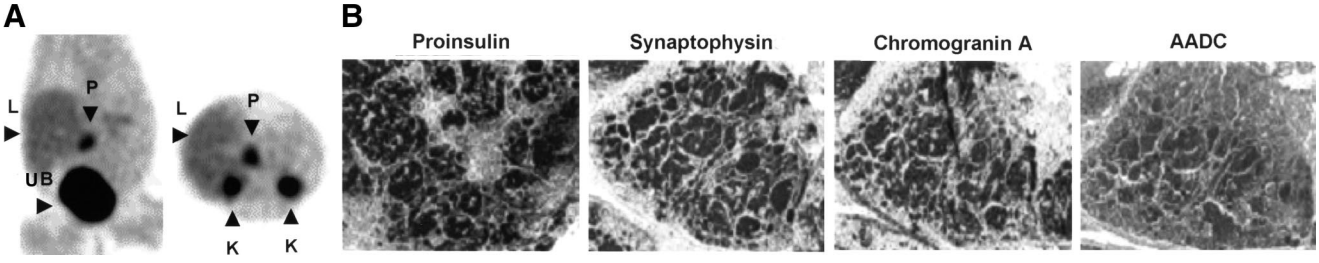

FIGURE 1. Patient with focal HI (patient 3). (A) Abnormal focal increased uptake of radiotracer is visualized in pancreas (P) on coronal and axial projections. Physiologic distribution of radiotracer with higher accumulation in kidneys (K) and urinary bladder (UB) and lower accumulation in liver (L) is also observed. (B) The 5 patients with focal HI forms were submitted to partial pancreatectomy. Abnormal hot spot corresponds to an important agglomeration of proinsulin, snaptophysin, chromogranin A, and AADC in adenoma (×100).

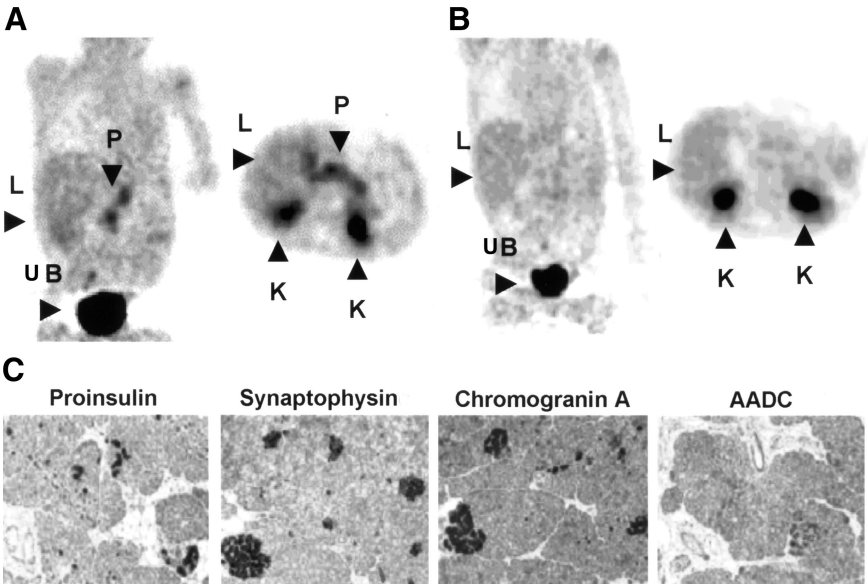

FIGURE 2. Patient with diffuse HI (patient 12). (A) Larger and diffuse uptake of radiotracer is observed over pancreatic area (P) (coronal and axial projections). Physiologic distribution of radiotracer with higher accumulation in kidneys (K) and urinary bladder (UB) and lower accumulation in liver (L) is also observed. (B) Images obtained for same patient after carbidopa administration: Note absence of ^{18}F-fluoro-L-DOPA uptake by pancreas. (C) Corresponding immunohistochemical results (proinsulin, snaptophysin, chromogranin A, and AADC) obtained for same patient after subtotal pancreatectomy (×100).

a complete clinical remission. In all 5 patients, the PET data were in accordance with immunohistochemical analysis. The abnormal β-cells, identified by their overexpression of proinsulin, synaptophysin, and chromogranin A, also overexpressed AADC (Fig. 1B, patient 3). The distribution of abnormal β-cells was restricted to the adenoma.

When a diffuse accumulation of ^{18}F-fluoro-L-DOPA (Fig. 2A, patient 12) was observed (n = 10), a diffuse HI was suspected, and the whole pancreas was resected if the patient was resistant to the medical treatment. Before subtotal pancrectomy, patient 12 was also treated with an inhibitor of AADC, carbidopa, which inhibits the conversion of ^{18}F-fluoro-L-DOPA to ^{18}F-fluoro-dopamine. The diffuse fixation without carbidopa disappeared completely under carbidopa treatment (Fig. 2B). In all patients who underwent surgical resection (n = 4), the PET results were confirmed by the histologic data. The abnormal pancreatic cells identified by their expression of proinsulin, synaptophysin, chromogranin A, and AADC were gathered in small clusters, scattered in the whole pancreas (Fig. 2C, patient 12).

No significant differences in ^{18}F-fluoro-L-DOPA uptake were observed between the 2 PET studies performed with and without octreotide and diazoxide (Figs. 3A and 3B).

The usefulness of coregistration images between PET and MRI is shown in Figure 4.

Throughout the whole acquisition, the ^{18}F-fluoro-L-DOPA biodistribution remained relatively stable over the pancreas, liver, and lungs, independent of the type of HI (Figs. 5A and 5B).

For each subject, the SUVs calculated for pancreas, liver, and lungs at 62.0 ± 4.5 min after injection are given in Table 2. The higher SUVs were observed for the pancreas, followed by the liver. The mean ± SD of SUVs were 2.2 ± 0.7 and 2.0 ± 0.6, respectively, for the pancreas hot spot in focal HI and pancreatic area in diffuse HI.

DISCUSSION

The present study showed that PET using ^{18}F-fluoro-L-DOPA positively differentiated between focal and diffuse HI. When a focal uptake of ^{18}F-fluoro-L-DOPA was detected, the immunohistochemical data obtained at the surgical resection always confirmed the diagnosis of focal HI. On the other hand, when a diffuse pattern of ^{18}F-fluoro-L-DOPA was observed, histologic data exhibited a large dispersion of the pathologic β-cells throughout the pancreas. The histologic findings corroborate the PET results and illustrate a pancreatic β-cell colocalization of proinsulin and AADC. Thus, the localization provided by PET seems to be as precise as that usually obtained by PVS and should be adequate to guide surgical resection in most cases.

For all 6 patients who underwent MRI, the images obtained did not distinguish between focal and diffuse disease. However, our study emphasized that coregistration of MRI with PET confirmed the radiopharmaceutical accumulation in the pancreas. Slight misregistrations due to the acquisition on separated imaging devices (different patient bed

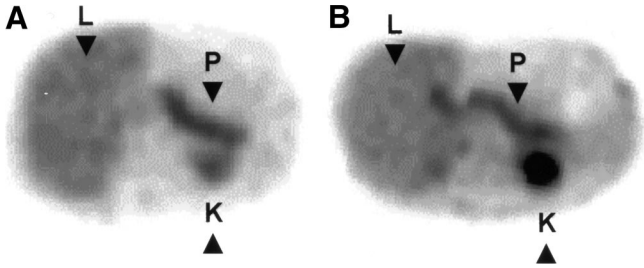

FIGURE 3. Axial slices obtained from patient 8 with diffuse HI. (A) Seventy-two hours after drug withdrawal. (B) Under administration of octreotide and diazoxide. No differences in ^{18}F-fluoro-L-DOPA pancreatic uptake were observed between the 2 PET studies. P = pancreas; L = liver; K = kidney.

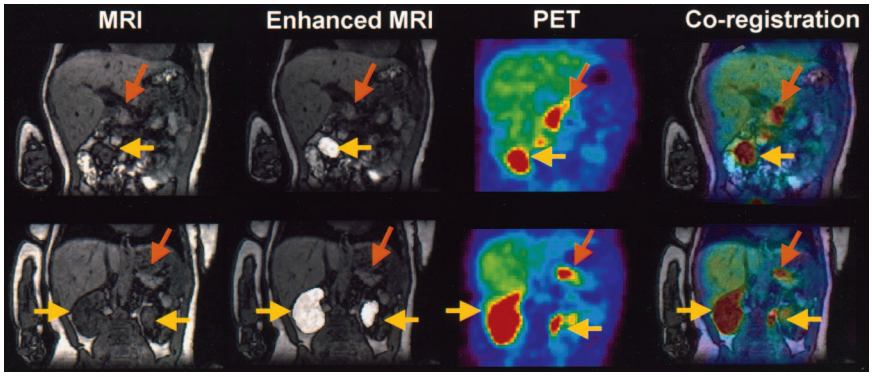

FIGURE 4. MRI, enhanced MRI, PET, and resultant coregistration images obtained from patient 8 with diffuse HI: Coregistration images confirm diffuse uptake of ^{18}F-fluoro-L-DOPA by pancreas (orange arrows = pancreas; yellow arrows = kidneys).

support) and to the softness of the tissues in the abdominal area have been observed (Fig. 4, coregistration images). However, the coregistration between MRI and PET images improves the localization of anatomic regions in PET as well the identification of the lesions.

The PET images showed that most of the injected radioactivity accumulated in the kidneys and urinary bladder, the main route of elimination of the radiotracer. Consequently, the high radioactivity concentrated in the kidneys—particularly in the left kidney—might make the identification of focal forms localized in the tail of the pancreas difficult.

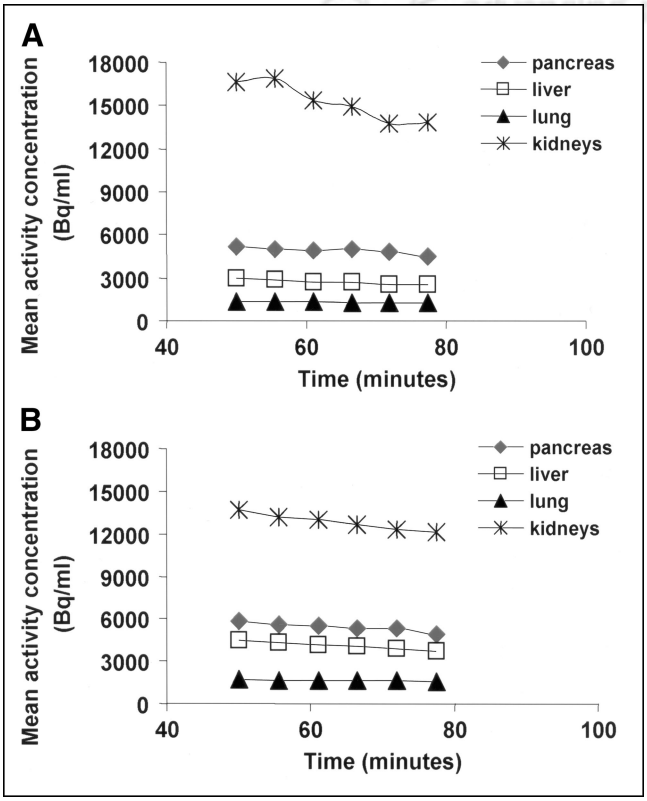

FIGURE 5. Time–activity curves (Bq/mL) in all measured organs between 50 and 80 min after intravenous injection of ^{18}F-fluoro-L-DOPA. Curves were obtained for a patient with focal HI (A) and a patient with diffuse HI (B).

The time–activity curves showed that the pancreatic radioactivity remained rather constant during the whole dynamic acquisition, independent of the type of HI. This result emphasizes that a 30-min dynamic acquisition is not useful; a 5-min scan should be informative enough. Furthermore, the emission acquisition could start between 45 and 90 min after injection. A similar observation was recently published in which ^{18}F-fluoro-L-DOPA was also used to study neuroendocrine tumors in adults (*36*).

We have used SUVs to distinguish the 2 forms of HI and to complete the visual inspection. However, although the pancreas SUVs seemed to be higher in focal HI than in diffuse HI, the difference was not statistically significant.

TABLE 2
Type of HI and Individual SUVs Measured 62.0 ± 4.5 Minutes After Injection

Patient no.	HI	SUV		
		Pancreas	Liver	Lung
1	Focal	1.7	0.9	0.5
2	Focal	1.5	1.1	0.5
3	Focal	2.1	1.4	0.6
4	Focal	2.5	1.7	0.4
5	Focal	3.3	1.1	0.4
6	Diffuse	2.5	1.5	0.6
7	Diffuse	2.1	1.6	0.6
8	Diffuse	2.4*	1.5*	0.5*
		2.0†	1.2†	0.4†
9	Diffuse	2.4	1.7	0.6
10	Diffuse	2.0	1.3	0.4
11	Diffuse	1.0	1.2	0.3
12	Diffuse	1.8	0.8*	0.3*
		ND‡	ND‡	ND‡
13	Diffuse	1.3	1.2	0.5
14	Diffuse	2.8	1.4	0.5
15	Diffuse	2.0	1.2	0.6

*PET acquisition after 72 h of drug withdrawal.
†PET acquisition under administration of octreotide and diazoxide.
‡PET acquisition after carbidopa administration.
ND = not determined.

This result may be due to the small number of patients with focal HI studied.

In patient 12, the diffuse ^{18}F-fluoro-L-DOPA uptake observed in the pancreas before treatment with carbidopa was no longer detectable after the administration of carbidopa. This result demonstrates, in vivo, that pancreas β-cells are able to take up L-DOPA, an amino precursor, and contain the enzyme AADC, which is responsible for the conversion of ^{18}F-fluoro-L-DOPA into ^{18}F-fluoro-dopamine. ^{18}F-Fluoro-L-DOPA is probably transported across the cell membrane by the amino acid transporter. Then it is decarboxylated into ^{18}F-fluoro-dopamine, which is stored in vesicles. When decarboxylation is prevented by an AADC inhibitor, such carbidopa, it is possible that ^{18}F-fluoro-L-DOPA is released from the tissue. Thus, the diffuse fixation shown by PET before treatment disappeared completely after the administration of carbidopa.

The effect of octreotide and diazoxide, medications generally used for HI, was tested in 1 patient (patient 8). The uptake of ^{18}F-fluoro-L-DOPA was unchanged. Thus, in contrast to PVS, PET studies could be performed without discontinuing the medication.

Surprisingly, when ^{11}C-L-DOPA was used instead of ^{18}F-fluoro-L-DOPA to detect pancreatic neuroendocrine tumors (*37,38*), only 1 of 3 insulinomas was diagnosed. One explanation might be that most adult insulinomas contain poorly differentiated β-cells with a low level of insulin synthesis and secretion. In contrast, in infantile hyperinsulinemic disease, the pancreatic β-cells are highly differentiated and hyperfunctioning.

CONCLUSION

Our results show that PET with ^{18}F-fluoro-L-DOPA is a promising method for the differential diagnosis between focal and diffuse HI. PET results are supported by the immunohistochemical analysis performed after partial (focal HI) or subtotal (diffuse HI resistant to medical treatment) pancreatectomy.

The localization provided by PET seems to be as precise as that obtained by PVS and, in most cases, should be enough to guide surgical resection. However, for focal HI localized at the tail of the pancreas, coregistration between PET and MR images appears to be necessary for optimal surgery planning.

ACKNOWLEDGMENTS

We are greatly indebted to the chemical and nursing staffs of Service Hospitalier Frédéric Joliot, Orsay, France. We are particularly grateful to Françoise Condé for histologic study assistance and to Christine Broissand, the Pharmacie Centrale des Hôpitaux de Paris, and the Institut des Maladies Rares (Paris) for the temporary agreement for the use of carbidopa. We also thank Dr. Ana Santos and Dr. Héric Valette for their critical reading of the manuscript.

REFERENCES

1. Stanley CA, Lieu YK, Hsu BY, et al. Hyperinsulinemia and hyperammonemia in infants with regulatory mutations of the glutamate dehydrogenase gene. *N Engl J Med.* 1998;338:1352–1357.
2. Menni F, de Lonlay P, Sevin C, et al. Neurologic outcomes of 90 neonates and infants with persistent hyperinsulinemic hypoglycemia. *Pediatrics.* 2001;107:476–479.
3. Rahier J, Falt K, Muntefering H, Becker K, Gepts W, Falkmer S. The basic structural lesion of persistent neonatal hypoglycaemia with hyperinsulinism: deficiency of pancreatic D cells or hyperactivity of B cells? *Diabetologia.* 1984;26:282–289.
4. Goossens A, Gepts W, Saudubray JM, et al. Diffuse and focal nesidioblastosis: a clinicopathological study of 24 patients with persistent neonatal hyperinsulinemic hypoglycemia. *Am J Surg Pathol.* 1989;13:766–775.
5. Thomas PM, Cote GJ, Wohllk N, et al. Mutations in the sulfonylurea receptor gene in familial persistent hyperinsulinemic hypoglycemia of infancy. *Science.* 1995;268:426–429.
6. Nestorowicz A, Wilson BA, Schoor KP, et al. Mutations in the sulfonylurea receptor gene are associated with familial hyperinsulinism in Ashkenazi Jews. *Hum Mol Genet.* 1996;5:1813–1822.
7. De Lonlay P, Fournet JC, Rahier J, et al. Somatic deletion of the imprinted 11p15 region in sporadic persistent hyperinsulinemic hypoglycemia of infancy is specific of focal adenomatous hyperplasia and endorses partial pancreatectomy. *J Clin Invest.* 1997;100:802–807.
8. Verkarre V, Fournet JC, de Lonlay P, et al. Paternal mutation of the sulfonylurea receptor (SUR1) gene and maternal loss of 11p15 imprinted genes lead to persistent hyperinsulinism in focal adenomatous hyperplasia. *J Clin Invest.* 1998;102:1286–1291.
9. Fournet JC, Mayaud C, de Lonlay P, et al. Unbalanced expression of 11p15 imprinted genes in focal forms of congenital hyperinsulinism: association with a reduction to homozygosity of a mutation in ABCC8 or KCNJ11. *Am J Pathol.* 2001;158:2177–2184.
10. De Lonlay-Debeney P, Poggi-Travert F, Fournet JC, et al. Clinical features of 52 neonates with hyperinsulinism. *N Engl J Med.* 1999;340:1169–1175.
11. Sempoux C, Guiot Y, Lefevre A, et al. Neonatal hyperinsulinemic hypoglycemia: heterogeneity of the syndrome and keys for differential diagnosis. *J Clin Endocrinol Metab.* 1998;83:1455–1461.
12. De Lonlay P, Benelli C, Fouque F, et al. Hyperinsulinism and hyperammonemia syndrome: report of twelve unrelated patients. *Pediatr Res.* 2001;50:353–357.
13. Hirsch HJ, Loo S, Evans N, Crigler JF, Filler RM, Gabbay KH. Hypoglycemia of infancy and nesidioblastosis: studies with somatostatin. *N Engl J Med.* 1977;296:1323–1326.
14. Glaser B, Hirsch HJ, Landau H. Persistent hyperinsulinemic hypoglycemia of infancy: long-term octreotide treatment without pancreatectomy. *J Pediatr.* 1993;123:644–650.
15. Thornton PS, Alter CA, Katz LE, Baker L, Stanley CA. Short- and long-term use of octreotide in the treatment of congenital hyperinsulinism. *J Pediatr.* 1993;123:637–643.
16. De Lonlay P, Fournet JC, Touati G, et al. Heterogeneity of persistent hyperinsulinaemic hypoglycaemia: a series of 175 cases. *Eur J Pediatr.* 2002;161:37–48.
17. Filler RM, Weinberg MJ, Cutz E, Wesson DE, Ehrlich RM. Current status of pancreatectomy for persistent idiopathic neonatal hypoglycemia due to islet cell dysplasia. *Prog Pediatr Surg.* 1991;26:60–75.
18. Fekete CN, de Lonlay P, Jaubert F, Rahier J, Brunelle F, Saudubray JM. The surgical management of congenital hyperinsulinemic hypoglycemia in infancy. *J Pediatr Surg.* 2004;39:267–269.
19. Brunelle F, Negre V, Barth MO, et al. Pancreatic venous samplings in infants and children with primary hyperinsulinism. *Pediatr Radiol.* 1989;19:100–103.
20. Dubois J, Brunelle F, Touati G, et al. Hyperinsulinism in children: diagnostic value of pancreatic venous sampling correlated with clinical, pathological and surgical outcome in 25 cases. *Pediatr Radiol.* 1995;25:512–516.
21. Chigot V, De Lonlay P, Nassogne MC, et al. Pancreatic arterial calcium stimulation in the diagnosis and localisation of persistent hyperinsulinemic hypoglycaemia of infancy. *Pediatr Radiol.* 2001;31:650–655.
22. Lemmer K, Ahnert-Hilger G, Hopfner M, et al. Expression of dopamine receptors and transporter in neuroendocrine gastrointestinal tumor cells. *Life Sci.* 2002;71:667–678.
23. Rodriguez MJ, Saura J, Finch CC, Mahy N, Billet EE. Localization of monoamine oxidase A and B in human pancreas, thyroid and adrenal glands. *J Histochem Cytochem.* 2000;48:147–151.
24. Orlefors H, Sundin A, Fasth KJ, et al. Demonstration of high monoaminoxi-

dase-A levels in neuroendocrine gastroenteropancreatic tumors in vitro and in vivo: tumor visualization using positron emission tomography with ^{11}C-harmine. *Nucl Med Biol.* 2003;30:669–679.
25. Oei HK, Gazdar AF, Minna JD, Weir GC, Baylin SB. Clonal analysis of insulin and somatostatin secretion and L-dopa decarboxylase expression by a rat islet cell tumor. *Endocrinology.* 1983;112:1070–1075.
26. Lindstrom P. Aromatic-L-amino-acid decarboxylase activity in mouse pancreatic islets. *Biochim Biophys Acta.* 1986;884:276–281.
27. Borelli MI, Villar MJ, Orezzoli A, Gagliardino JJ. Presence of DOPA decarboxylase and its localisation in adult rat pancreatic islet cells. *Diabetes Metab.* 1997;23:161–163.
28. Hoegerle S, Altehoefer C, Ghanem N, et al. Whole-body ^{18}F DOPA PET for detection of gastrointestinal carcinoid tumors. *Radiology.* 2001;220:373–380.
29. Hoegerle S, Nitzche E, Altehoefer C, et al. Pheochromocytomas: detection with ^{18}F DOPA whole-body PET: initial results. *Radiology.* 2002;222:507–512.
30. Dollé F, Demphel S, Hinnen F, Fournier D, Vaufrey F, Crouzel C. 6-[^{18}F]Fluoro-L-DOPA by radiofluorodestannylation: a short and simple synthesis of a new labelling precursor. *J Labelled Compds Radiopharm.* 1998;XLI:105–114.
31. Wells WM, Viola PV, Atsumi H, Nakajima S, Kikinis R. Multi-modal volume registration by maximization of mutual information. *Med Image Anal.* 1996;1:35–51.
32. Maes F, Collignon A, Vandermeulen D, Marechal G, Suetens R. Multimodality image registration by maximization of mutual information. *IEEE Trans Med Imaging.* 1997;16:187–198.
33. Pulim JPW, Maintz JBA, Viergever MA. Mutual information based registration of medical images: a survey. *IEEE Trans Med Imaging.* 2003;22:986–1004.
34. Maintz J, Viergever M. A survey for medical image registration. *Med Image Anal.* 1998;2:1–36.
35. Lemke AJ, Niehues SM, Hosten N, et al. Retrospective digital image fusion of multidetector CT and ^{18}F-FDG PET: clinical value in pancreatic lesions—a prospective study with 104 patients. *J Nucl Med.* 2004;45:1279–1286.
36. Becherer A, Szabo M, Karanikas G, et al. Imaging of advanced neuroendocrine tumors with ^{18}F-FDOPA PET. *J Nucl Med.* 2004;45:1161–1167.
37. Ahlstrom H, Eriksson B, Bergstrom M, Bjurling P, Langstrom B, Oberg K. Pancreatic neuroendocrine tumors: diagnosis with PET. *Radiology.* 1995;195:333–337.
38. Bergstrom M, Eriksson B, Oberg K, et al. In vivo demonstration of enzyme activity in endocrine pancreatic tumors: decarboxylation of carbon-11-DOPA to carbon-11-dopamine. *J Nucl Med.* 1996;37:32–37.